AASLD
AMERICAN ASSOCIATION FOR
THE STUDY OF LIVER DISEASES

ORIGINAL ARTICLE

Essential lipid autacoids rewire mitochondrial energy efficiency in metabolic dysfunction-associated fatty liver disease

Cristina López-Vicario[1,2,3] | David Sebastián[4,5] | Mireia Casulleras[1,3] |
Marta Duran-Güell[1,3] | Roger Flores-Costa[1,3] | Ferran Aguilar[3] |
Juan José Lozano[2] | Ingrid W. Zhang[1,3] | Esther Titos[1,2,6] | Jing X. Kang[7] |
Antonio Zorzano[4,5] | Makoto Arita[8,9] | Joan Clària[1,2,3,6]

[1]Biochemistry and Molecular Genetics Service, Hospital Clínic, Institut D'Investigacions Biomèdiques August Pi i Sunyer, Barcelona, Spain

[2]Centro de Investigación Biomédica en Red de Enfermedades Hepáticas y Digestivas, Barcelona, Spain

[3]European Foundation for the Study of Chronic Liver Failure and Grifols Chair, Barcelona, Spain

[4]Institute for Research in Biomedicine, The Barcelona Institute of Science and Technology, Departament de Bioquímica i Biomedicina Molecular, University of Barcelona, Barcelona, Spain

[5]Centro de Investigación Biomédica en Red de Diabetes y Enfermedades Metabólicas Asociadas, Madrid, Spain

[6]Department of Biomedical Sciences, University of Barcelona, Barcelona, Spain

[7]Laboratory for Lipid Medicine and Technology, Massachusetts General Hospital and Harvard Medical School, Boston, Massachusetts, USA

[8]Laboratory for Metabolomics, RIKEN Center for Integrative Medical Sciences, Yokohama, Japan

[9]Division of Physiological Chemistry and Metabolism, Graduate School of Pharmaceutical Sciences, Keio University, Tokyo, Japan

Correspondence
Cristina López-Vicario and Joan Clària, Department of Biochemistry and Molecular Genetics, Hospital Clínic, Villarroel 170, Barcelona 08036, Spain.
Email: clopezv@recerca.clinic.cat and jclaria@clinic.cat

Abstract

Background and Aim: Injury to hepatocyte mitochondria is common in metabolic dysfunction-associated fatty liver disease. Here, we investigated whether changes in the content of essential fatty acid–derived lipid autacoids affect hepatocyte mitochondrial bioenergetics and metabolic efficiency.

Approach and Results: The study was performed in transgenic mice for the *fat-1* gene, which allows the endogenous replacement of the membrane omega-6–polyunsaturated fatty acid (PUFA) composition by omega-3–PUFA. Transmission electron microscopy revealed that hepatocyte mitochondria of *fat-1* mice had more abundant intact cristae and higher mitochondrial aspect ratio. *Fat-1* mice had increased expression of oxidative phosphorylation complexes I and II and translocases of both inner (translocase of inner mitochondrial

Abbreviations: AA, arachidonic acid; ADP, adenosine diphosphate; AKT, serine/threonine protein kinase; ATP, adenosine triphosphate; BMP, bis(monoacylglycero)phosphate; CDAHFD, choline-deficient L-amino acid–defined HFD; DHA, docosahexaenoic acid; EPA, eicosapentaenoic acid; ETC, electron transport chain; eWAT, epididymal white adipose tissue; FA, fatty acid; FAO, FA β-oxidation; HDHA, hydroxy-DHA; HFD, high-fat diet; iBAT, interscapular brown adipose tissue; LA, linoleic acid; MaR1, maresin 1; OCR, enhanced oxygen consumption rate; OXPHOS, oxidative phosphorylation; PC, phosphatidylcholine; PE, phosphatidylethanolamine; PG, phosphatidylglycerol; PI, phosphatidylinositol; PS, phosphatidylserine; PUFA, polyunsaturated fatty acid; ROS, radical oxygen species; RvD1, resolvin D1; SI, supporting information; TAG, triglyceride; TCA, tricarboxylic acid; TEM, transmission electron microscopy; TIM44, translocase of inner mitochondrial membrane 44; WT, wild-type.

membrane 44) and outer (translocase of the outer membrane 20) mitochondrial membranes. *Fat-1* mice also showed increased mitofusin-2 and reduced dynamin-like protein 1 phosphorylation, which mediate mitochondrial fusion and fission, respectively. Mitochondria of *fat-1* mice exhibited enhanced oxygen consumption rate, fatty acid β-oxidation, and energy substrate utilization as determined by high-resolution respirometry, [1-^{14}C]-oleate oxidation and nicotinamide adenine dinucleotide hydride/dihydroflavine-adenine dinucleotide production, respectively. Untargeted lipidomics identified a rich hepatic omega-3−PUFA composition and a specific docosahexaenoic acid (DHA)−enriched lipid fingerprint in *fat-1* mice. Targeted lipidomics uncovered a higher content of DHA-derived lipid autacoids, namely resolvin D1 and maresin 1, which rescued hepatocytes from TNFα-induced mitochondrial dysfunction, and unblocked the tricarboxylic acid cycle flux and metabolic utilization of long-chain acyl-carnitines, amino acids, and carbohydrates. Importantly, *fat-1* mice were protected against mitochondrial injury induced by obesogenic and fibrogenic insults.

Conclusion: Our data uncover the importance of a lipid membrane composition rich in DHA and its lipid autacoid derivatives to have optimal hepatic mitochondrial and metabolic efficiency.

INTRODUCTION

Mitochondria are the cell powerhouse and are entrusted with the challenging task of providing energy to the cell through the generation of adenosine triphosphate (ATP).[1] Hepatocytes are rich in mitochondria, and the liver is a key insulin-sensitive organ coordinating and fine-tuning the complex network(s) of human metabolism.[2] At present, there is accumulating evidence that mitochondria are central organelles in the pathogenesis of metabolic dysfunction-associated liver disease.[3] In fact, defective mitochondrial electron transport chain (ETC) and impaired free fatty acid (FA) β-oxidation, together with excessive generation of radical oxygen species (ROS) and lipid peroxidation, play key roles in the development of persistent inflammation, increased oxidative stress and extensive liver cell injury, and progression to liver fibrosis and, ultimately, to liver cirrhosis.[4,5] Based on these findings, any approach to improve mitochondrial function or to protect hepatocytes from mitochondrial damage is of major interest for preventing liver-related metabolic dysfunctions.

The lipid composition of mitochondrial membranes is essential for the function of these cellular organelles.[6] Mitochondrial membranes are enriched with phospholipid species such as phosphatidylcholine (PC), phosphatidylethanolamine (PE), phosphatidylinositol (PI), phosphatidylserine (PS), and cardiolipin.[6] Essential FAs, especially polyunsaturated FA (PUFA) esterified into membrane phospholipids, are critical for optimal lipid molecular organization, lipid microenvironment, and mitochondrial function, including the respiratory enzymes involved in oxidative phosphorylation (OXPHOS).[7] PUFAs are classified into two families, namely omega-6 and omega-3, with diverse effects on mitochondrial membrane homeostasis. For instance, the omega-6−PUFA arachidonic acid (AA) biosynthesized from the conversion of linoleic acid (LA) through desaturation and elongation reactions can replace LA in the mitochondrial membrane. This replacement leads to changes in membrane permeability, impaired function of respiratory chain complexes, generation of ROS, and mitochondrial depolarization through an uncoupling effect that dissociates ETC from the production of ATP.[8,9] In contrast, the omega-3−PUFAs eicosapentaenoic acid (EPA) and docosahexaenoic acid (DHA) might improve mitochondrial adenosine diphosphate (ADP) kinetics by displacing omega-6−PUFAs in phospholipids.[10] Omega-3−PUFAs can also reduce hydrogen peroxide and ROS production[11,12] and increase the ETC coupling efficiency.[13] Importantly, essential omega-3−PUFAs are biosynthetically converted to lipid autacoids with potent pro-resolving properties, which have been reported to attenuate mitochondrial dysfunction and tissue/organ injury.[14−16]

The aim of the current investigation was to explore the impact of omega-3−PUFA enrichment on mitochondrial function using *fat-1* mice. These transgenic mice express an omega-3 desaturase encoded by the

fat-1 gene from *Caenorhabditis elegans* that allows endogenous conversion of omega-6 into omega-3–PUFA.[17–19] *Fat-1* mice possess a high omega-3–PUFA content in cell membrane phospholipids, evading any confounding factor inherent to the supplementation of PUFAs through the diet. In addition, *fat-1* mice are endogenously enriched with omega-3–derived lipid autacoids.[20,21] In this study, we investigated the constitutive mitochondrial phenotype (i.e., mitochondrial ultrastructure, OXPHOS, FA β-oxidation [FAO], and metabolic fluxes) in hepatocytes from *fat-1* mice. We also performed *in vitro* experiments to test whether omega-3–PUFA-derived autacoids protect hepatocytes from TNFα-induced mitochondrial dysfunction and whether *fat-1* mice are more resistant *in vivo* to obesogenic and fibrogenic induction models.

MATERIALS AND METHODS

Generation of fat-1 mice colonies and DNA genotyping

Hemizygous *fat-1* mice were generated and backcrossed onto a C57BL/6 background and genotyped by capillary electrophoresis as previously described[17,19] and as detailed in the online Supporting Information (SI). All animal studies were conducted in accordance with the criteria of the Investigation and Ethics Committee of the University of Barcelona (Barcelona, Spain) following the EU laws governing the use of experimental animals.

Experimental studies

Studies in male *fat-1* (*n* = 26) and wild-type (WT; *n* = 33) mice were conducted in accordance with the criteria of the Investigation and Ethics Committee of the University of Barcelona. At 6 weeks of age, mice were placed on either a standard rodent chow diet (13% kcal from fat), a high-fat diet (HFD; custom diet D09031101, 60% kcal from fat), or a choline-deficient L-amino acid–defined HFD (CDAHFD) (all from Research Diets, New Brunswick, NJ) for 24 weeks. At the end of the intervention period, the liver, interscapular brown adipose (iBAT), and epididymal white adipose tissues (eWATs) were collected (see online SI).

Histological analysis

Liver samples were fixed in 10% formalin and embedded in paraffin or fixed in methylbutane and embedded in optimal cutting temperature compound and sections stained with hematoxylin and eosin (H&E), Masson's trichrome, and oil red-O (see online SI).

Biochemical analyses

Serum concentrations of alanine aminotransferase (ALT) and aspartate amino transferase (AST) were determined using the Dri-Chem NX600 equipment (Fujifilm, Tokyo, Japan). Triglyceride (TAG) levels were determined using a TAG colorimetric assay kit (Cayman Chemical, Ann Harbor, MI).

Transmission electron microscopy

Mice livers were washed by perfusion procedure with cold Hanks' Balance Salt Solution without calcium/magnesium and fixed using 2.5% glutaraldehyde and 2% paraformaldehyde in phosphate buffer (0.1 M [pH 7.4]). Liver tissue fragments were postfixed in 1% osmium tetroxide, which is an excellent fixative to visualize the lipids of the membranous structures and vesicles,[22] and 0.8% potassium ferrocyanide; dehydrated with acetone; and embedded in epoxy resin (Spurr). Ultrathin sections were cut for transmission electron microscopy (TEM) and stained with 2% uranyl acetate and a lead-staining solution, and images acquired using the JEOL JEM-1010. See online SI.

Isolation and incubation of primary hepatocytes

Hepatocytes were isolated from WT (*n* = 10) and *fat-1* (*n* = 6) mice by a three-step in situ perfusion procedure using 0.03% collagenase IV (Sigma-Aldrich, St. Louis, MO) through the portal vein, as previously described[18] (see online SI).

Isolation of mitochondria

Five hundred milligrams of liver were homogenized using a polytetrafluoroethylene pestle in ice-cold buffer (250 mM sucrose, 50 mM KCl, 5 mM EDTA, 5 mM $MgCl_2$, and 1 mM $Na_4P_2O_7$, protease inhibitor [Complete Mini; Roche, Basel, Switzerland] at pH 7.4) and centrifuged at 740 × *g* for 5 min at 4°C. Supernatants were centrifuged at 9000 × *g* for 15 min at 4°C. The pellet was resuspended in 1000 μl of ice-cold buffer and centrifuged again at 10,000 × *g* for 15 min at 4°C. The final mitochondria-enriched pellet was resuspended in 500–1000 μl of ice-cold buffer and used for the measurement of FAO and oxygen consumption.

Measurement of oxygen consumption in isolated mitochondria

Respiration of isolated mitochondria was measured at 37°C by high-resolution respirometry with

the Oxygraph-2k (Oroboros Instruments, Innsbruck, Austria), as detailed in the online SI.

Measurement of FAO in isolated mitochondria

FAO was assessed by measuring oleate oxidation in mitochondrial enriched fractions, as detailed in the online SI.

Mitochondrial metabolic flux analysis

Mitochondrial flux analysis in primary hepatocytes was performed using MitoPlate S-1 plates (Biolog, Hayward, CA). See online SI for details.

RNA extraction, reverse transcription, and real-time polymerase chain reaction

Total RNA from the liver, iBAT and eWAT was extracted using the TRIzol reagent and after cDNA synthesis real-time polymerase chain reaction amplifications were carried out in an ABI Prism 7900HT Sequence Detection System (see online SI).

Analysis of protein expression by western blot

Total protein expression of translocase of inner mitochondrial membrane 44 (TIM44), translocase of the outer membrane 20 (TOM20), mitofusin 2 (MFN2), optic atrophy protein 1, phosphorylated dynamin-like protein 1 and total dynamin-like protein 1 (DLP1), and phosphorylated serine/threonine protein kinase (AKT) and total AKT were performed from liver extracts by western blot method. Expression of OXPHOS complexes I–V was assessed using the OXPHOS antibody cocktail. The glyceraldehyde 3-phosphate dehydrogenase protein expression was used as housekeeping signal (see online SI).

Lipid extraction

Lipids were extracted from liver tissues using single-phase extraction. Briefly, liver tissue homogenates were mixed with methanol (MeOH) and incubated for 1 h at room temperature. A half volume of $CHCl_3$ was added, and samples were incubated for 1 h at room temperature. Finally, water was added, and extracts composed of MeOH:$CHCl_3$:H_2O (2:1:0.2; vol/vol) were obtained. After extraction, samples were centrifuged at 2000 × g for 10 min, and the supernatants were collected.

Untargeted liquid chromatography–tandem mass spectrometry lipidomics

Untargeted analysis from lipid extracts was performed using an ACQUITY ultra performance liquid chromatography system (Waters, Milford, MA) coupled with a quadrupole time-of-flight/mass spectrometry (MS) (Triple time-of-flight 5600+, SCIEX, Framingham, MA) as previously described[23,24] (see online SI).

Targeted liquid chromatography–tandem MS lipidomics

The targeted analysis was performed as described previously[24] (see online SI).

Statistical analysis

All analysis and computations were performed using GraphPad v6.0 and R v4.0.2 (see online SI).

RESULTS

Distinct mitochondrial TEM ultrastructure of hepatocytes from *fat-1* mice

We first analyzed the mitochondrial ultrastructure of liver cells from *fat-1* and WT mice by TEM. Figure 1A shows TEM images from ultrathin sections of fixative-perfused livers showing binucleated hepatocytes with a well-defined nucleus perimeter and plasma membrane border, glycogen granules (dark granules), and numerous uniform mitochondria with normal cristae. Digitally colored TEM images revealed that as compared with WT, mitochondria from *fat-1* mice exhibited relatively more intact cristae (Figure 1B). The number of mitochondria per field and the Feret's diameter were not different between *fat-1* and WT mice (Figure 1C). In contrast, the mitochondrial aspect ratio (the ratio between the major and minor axis of the ellipse equivalent to the mitochondrion) was significantly higher in *fat-1* mice than WT (Figure 1D), suggesting improved mitochondrial fission/fusion balance for optimal structure/shape and function.[14,25–27] Improved mitochondrial fission/fusion balance was confirmed by western blot, showing increased MFN2 levels and decreased DLP1 phosphorylation in livers from *fat-1* mice (Figure 1E). Furthermore, *fat-1* mice showed increased levels of the outer membrane protein TOM20 as well as higher expression of the essential inner membrane protein TIM44 and OXPHOS complexes I and II (Figure 1F,G). Together, these findings led us to hypothesize that *fat-1* mice might have a higher liver mitochondrial capacity.
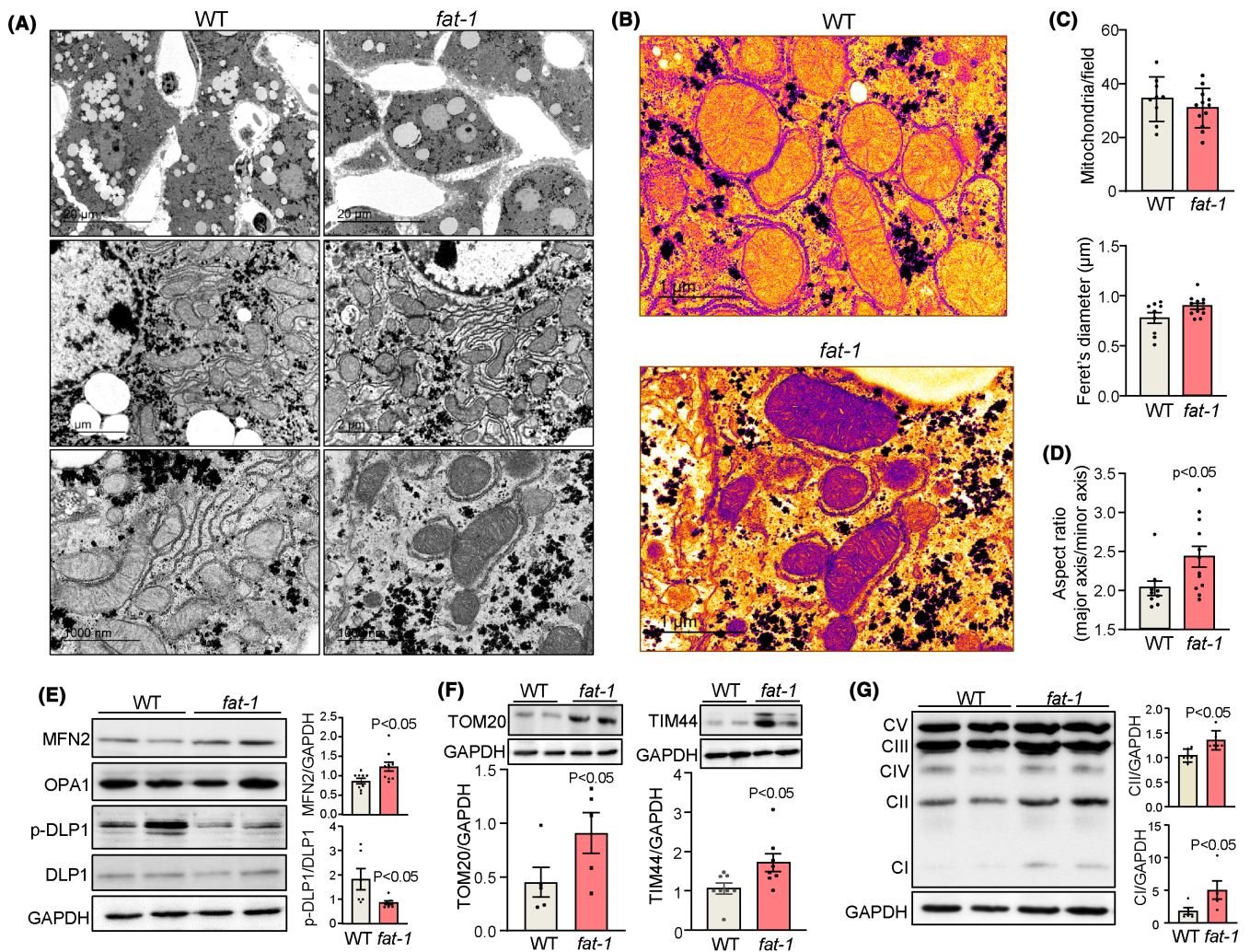
FIGURE 1 Mitochondria ultrastructure in hepatocytes enriched in omega-3 polyunsaturated fatty acid. (A) Representative transmission electron microscopy (TEM) images of ultrathin liver sections from wild-type (WT) ($n = 3$) and *fat-1* ($n = 3$) mice at magnifications of 3000× (upper panels), 20,000× (medium panels), and 50,000× (lower panels). (B) Digitally colored TEM images of ultrathin liver sections from WT and *fat-1* mice at 40,000× magnification. (C) Number of mitochondria per field and Feret's diameter. (D) Aspect ratio (major axis/minor axis) of each mitochondrion. (E) Western blot analysis of mitofusin 2 (MFN2), optic atrophy protein 1 (OPA1), phosphorylated dynamin-like protein 1 (p-DLP1), dynamin-like protein 1 (DLP1), and glyceraldehyde 3-phosphate dehydrogenase (GAPDH) in liver tissue from WT ($n = 8$) and *fat-1* ($n = 8$) mice. Densitometry of MFN2 signal normalized to GAPDH (upper graph) and p-DLP1 signal normalized to total DLP1 (lower graph). (F) Western blot analysis of translocase of the outer membrane 20 (TOM20), translocase of inner mitochondrial membrane 44 (TIM44), and GAPDH in livers from WT and *fat-1* mice. Representative blot images and normalization of signals with respect to GAPDH are shown below. (G) Representative blot images of hepatic expression of mitochondrial electron transport chain proteins (complex I [CI; NDUFB8], complex II [CII; SDHB], complex III [CIII; UQCRC2], complex IV [CIV; MTCO1], and complex V [CV; adenosine triphosphate 5A (ATP5A)]) and GAPDH in WT and *fat-1* mice. The quantification of CI and CII signals normalized to GAPDH are shown on the right. ATP5A, ATP synthase subunit alpha; MTCO1, cytochrome c oxidase subunit 1; NDUFB8, NADH dehydrogenase beta subcomplex subunit 8; SDHB, succinate dehydrogenase subunit B; UQCR2, cytochrome b-c1 complex subunit 2.

Enhanced oxygen consumption rate by mitochondria from *fat-1* mice

To confirm this hypothesis, we isolated hepatic mitochondria from *fat-1* and WT mice and measured oxygen consumption by high-resolution respirometry. This parameter was assessed by titration of different mitochondrial substrates, protein uncouplers, and inhibitors of the ETC, as schematized in Figure 2A. Representative respirometry curves from WT and *fat-1* mice under resting conditions are shown in Figure S1A. Mitochondria

from *fat-1* and WT mice had similar respiration in the absence of OXPHOS (LEAK), as determined by the addition of the complex I substrates glutamate/malate (GM) (Figure 2B). The addition of ADP to GM (GM/ADP [GMD]), which allows the coupling of OXPHOS to ATP production and the subsequent addition of succinate (GMD/succinate), as a substrate of complex II to generate dihydroflavine-adenine dinucleotide (FADH$_2$), resulted in an increased enhanced oxygen consumption rate (OCR) in both groups of mice; this effect being more pronounced in *fat-1* (Figure 2B). The addition of the
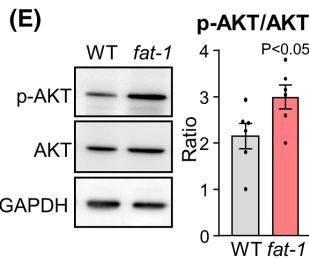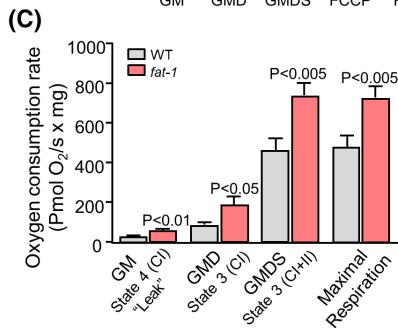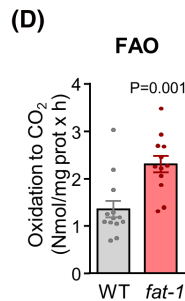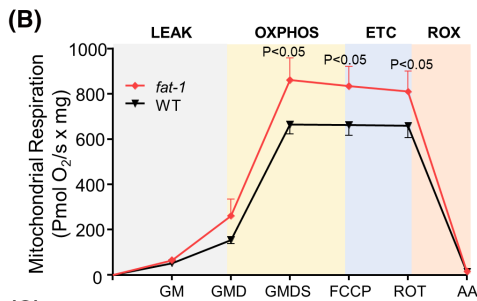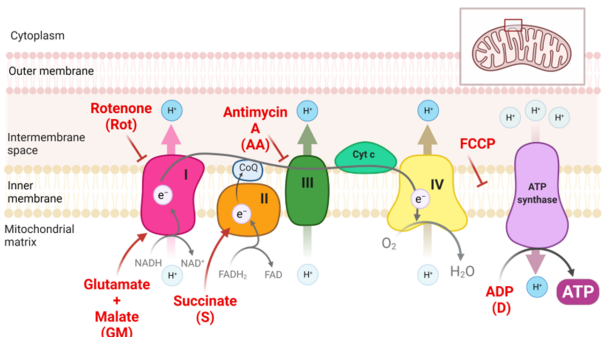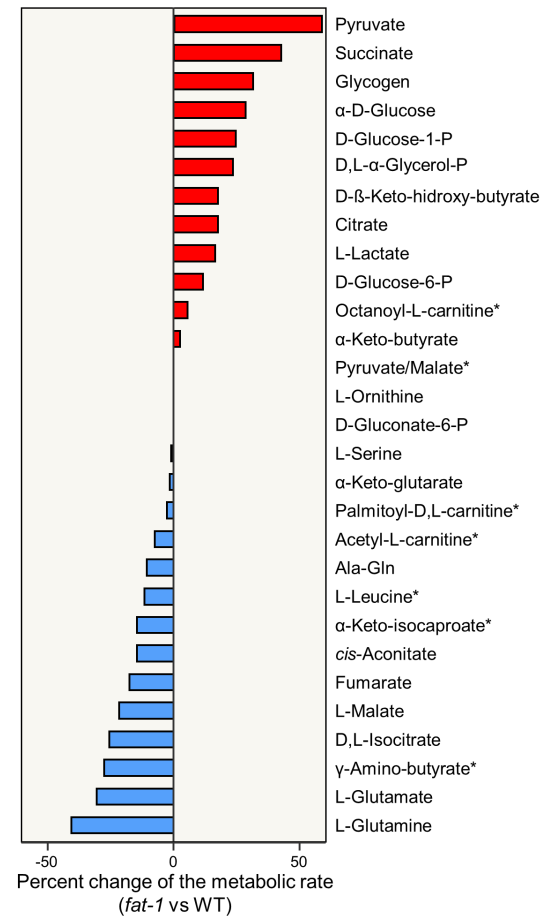
FIGURE 2 Enhanced respiration, fatty acid β-oxidation (FAO), insulin sensitivity, and energy substrate utilization in mitochondria from hepatocytes enriched in omega-3 polyunsaturated fatty acid. (A) Schematic diagram of substrates, protein uncouplers, and inhibitors of mitochondrial electron transport chain (ETC). (B) Oxygen consumption rate (OCR) of isolated mitochondria from livers of wild-type (WT) ($n = 9$) and *fat-1* ($n = 11$) mice as measured by high-resolution respirometry using the substrate/inhibitor titration protocol. (C) OCR values corrected by residual oxygen consumption (ROX). (D) Measurements of radiolabeled [1-^{14}C]-oleate FAO of isolated mitochondria from livers of WT ($n = 13$) and *fat-1* ($n = 12$) mice. (E) Representative blot images of phosphorylated serine/threonine protein kinase (p-AKT), total serine/threonine protein kinase (AKT), and glyceraldehyde 3-phosphate dehydrogenase proteins and p-AKT/AKT ratio in liver tissue from WT ($n = 8$) and *fat-1* ($n = 8$) mice. (F) Bar plot showing the ranked percent change in metabolic rate for each substrate of mitochondrial/glycolytic pathways in primary hepatocytes from *fat-1* ($n = 6$) mice with respect to WT ($n = 10$). Hepatocytes were cultured in the plate for 12 h, and the data were normalized by the cell number as well as by the intensity of the succinate signal of each experiment to reduce batch-effects. Malate was added at a concentration of 100 μM to these substrates. AA, antimycin A; ADP, adenosine diphosphate; ATP, adenosine triphosphate; CI, complex I; CII, complex II; Cyt c, cytochrome c; FAD, flavin adenine dinucleotide; FADH$_2$, dihydroflavine-adenine dinucleotide; FCCP, carbonylcyanide-4-(trifluoromethoxy)-phenylhydrazone; GM, glutamate/malate; GMD, GM/adenosine diphosphate; GMDS, GMD/succinate; NAD, nicotinamide adenine dinucleotide; NADH, nicotinamide adenine dinucleotide hydride; OXPHOS, oxidative phosphorylation; ROT, rotenone; S, succinate.

mitochondrial uncoupler protonophore carbonylcyanide-4-(trifluoromethoxy)-phenylhydrazone, which dissipates mitochondrial membrane potential, also resulted in a significantly higher OCR in *fat-1* than WT mice (Figure 2B). The consumption in the uncoupled state because of complex II activity, determined by inhibiting complex I with the addition of rotenone, was also higher in *fat-1* mice. Finally, electron transport through complex III was inhibited in both groups of mice by adding antimycin A to obtain the levels of residual oxygen consumption that allowed the correction of OCR data (Figure 2C).

Taken together, the presence of higher OCR in *fat-1* mice confirmed the enhanced proficiency of their liver mitochondria.

Enhanced mitochondrial FAO, insulin sensitivity, and energy substrate utilization in *fat-1* mice

We next performed experiments with [1-^{14}C]-oleate to assess FAO, another key mitochondrial process. *Fat-1*

mice hepatocyte mitochondria showed increased FAO with respect to WT mice (Figure 2D). *Fat-1* mice also showed increased liver AKT phosphorylation at serine 473, suggesting enhanced glucose and lipid metabolism in this insulin-sensitive tissue (Figure 2E). To further explore this observation, we performed metabolic flux analysis from different substrates of mitochondrial/glycolytic pathways in hepatocytes by measuring the electron flow rates into and through the ETC. Consistent with higher AKT phosphorylation, hepatocytes from *fat-1* mice showed increased metabolic rate for carbohydrates (i.e., pyruvate, glucose, and glucose-derived products) (Figure 2F). *Fat-1* mice also showed enhanced utilization of tricarboxylic acid (TCA) cycle intermediates such as succinate and citrate to produce nicotinamide adenine dinucleotide hydride and $FADH_2$ to feed the ETC (Figure 2F).

Identification of a specific DHA-enriched lipid fingerprint in *fat-1* mice

Lipids, especially PUFAs, are highly important for numerous mitochondrial functions.[6] Consequently, we assessed the hepatic PUFA content in *fat-1* and WT mice by targeted lipidomics. As expected and consistent with previous findings,[18] livers from *fat-1* mice presented increased levels of omega-3–PUFAs (i.e., EPA, docosapentaenoic acid [DPA] omega-3 and DHA) with few variations in the content of the omega-6–PUFA AA (Figure 3A). Consistently, *fat-1* mice had a reduced omega-6/omega-3 ratio (Figure 3B) and an increased omega-3 index (total content of EPA and DHA) (Figure 3C). The omega-3-PUFA linolenic and other less abundant omega-3–PUFAs were also increased in *fat-1* mice (Figure S2A), whereas the omega-6–PUFAs adrenic and osbond acids were decreased (Figure S2B). The content of saturated and monounsaturated FAs was similar in both groups of mice (Figure S2C). To obtain deeper insight into the lipid composition of *fat-1* mice, we performed untargeted lipidomics employing liquid chromatography–tandem MS (LC–MS/MS). This untargeted analysis unambiguously identified 281 lipid species in the liver of *fat-1* and WT mice (Table S1). By grouping these lipids by class and graphing their percentual contribution to the whole liver lipid pool, we observed that liver tissue in both groups of mice was mostly enriched in phospholipids [from more to less abundant: PC, PE, PI, phosphatidylglycerol (PG), and its structural isomer bis(monoacylglycero)phosphate (BMP) and PS] (Figure 3D). See Figure S3 for a schematic representation of the phospholipid pathway in the liver. The percentual distribution of these phospholipid families was similar in *fat-1* and WT mice, but the total content of PE and PS was higher in *fat-1* mice, as shown in the lollipop chart in Figure 3E. The representation in a circos plot of the fold changes in each individual phospholipid between *fat-1* and WT mice revealed that the FA content of *fat-1* phospholipids was largely dominated by omega-3–PUFAs (Figure 3F). The highest fold changes were seen in PG as well as in BMP, which have the peculiarity of being naturally enriched in DHA[28] (Figure 3F). Furthermore, grouping phospholipids by subfamily and their PUFA content, we identified that the most abundant phospholipids in *fat-1* mice, namely PC and PE, were mostly enriched in DHA (Figure S3).

We next performed explorative multivariate analysis of the untargeted lipidomics data using PCA. As shown in the score plot in Figure 4A, WT and *fat-1* mice had distinct clustering with PC1 and PC2 values of 50.6% and 18.3%, respectively. By computing fold changes for each lipid species in *fat-1* with respect to WT mice and generating a heatmap of lipids with significant FDR, we identified two clusters: cluster 1 composed of 36 lipids, the levels of which were lower in *fat-1* compared with WT mice; and cluster 2, which included 36 lipids with higher abundance in *fat-1* mice (Figure 4B). See Table S1 for details of the fold changes and FDR for these lipids. Importantly, the lipids included in cluster 1 (reduced amount in *fat-1* mice) contained at least one omega-6–PUFA, either AA, osbond acid, or LA (Figure 4B), whereas lipids included in cluster 2 (increased amount in *fat-1* mice) were enriched in omega-3–PUFAs, especially DHA (Figure 4B). To reduce the dimension of this lipid data set, we created a volcano plot considering the extent of both fold changes and statistical significance (*p* values) between *fat-1* and WT mice (Figure 4C). The 10 lipid species with the highest positive fold changes with statistically significant values were phospholipids enriched in DHA, including PG(22:6/22:6), BMP(22:6/22:6), PG(20:3/22:6), lysophosphatidylglycerol (22:6), PI(18:0/22:6), PG(22:4/22:6), BMP(18:2/22:6), PG(18:2/22:6), PG(20:4/22:6), and PS(16:0/22:6) (Figure 4C and Table S1). In contrast, the 10 lipid species with the highest negative fold changes and statistically significant values were enriched with the omega-6 osbond acid and some with the omega-6 AA (i.e., PG[22:5/22:5], BMP[22:5/22:5], lysophosphatidylethanolamine[22:5], PE[18:1/22:5], BMP[20:4/22:5], PE[16:0/22:5], lysophosphatidylcholine[22:5], PG[20:4/22:5], PC[18:1/22:5], and PC[20:4/22:5]) (Figure 4C and Table S1). Together, these findings indicate that livers from *fat-1* mice have an enriched composition of phospholipids containing the omega-3–PUFA DHA.

DHA-derived lipid autacoids protect hepatocytes from TNFα-induced mitochondrial dysfunction

DHA, as well as other omega-3–PUFAs such as EPA and DPA, are precursors of bioactive lipid autacoids, which actively promote the resolution of inflammation and protect tissues against injury.[29] Accordingly, we
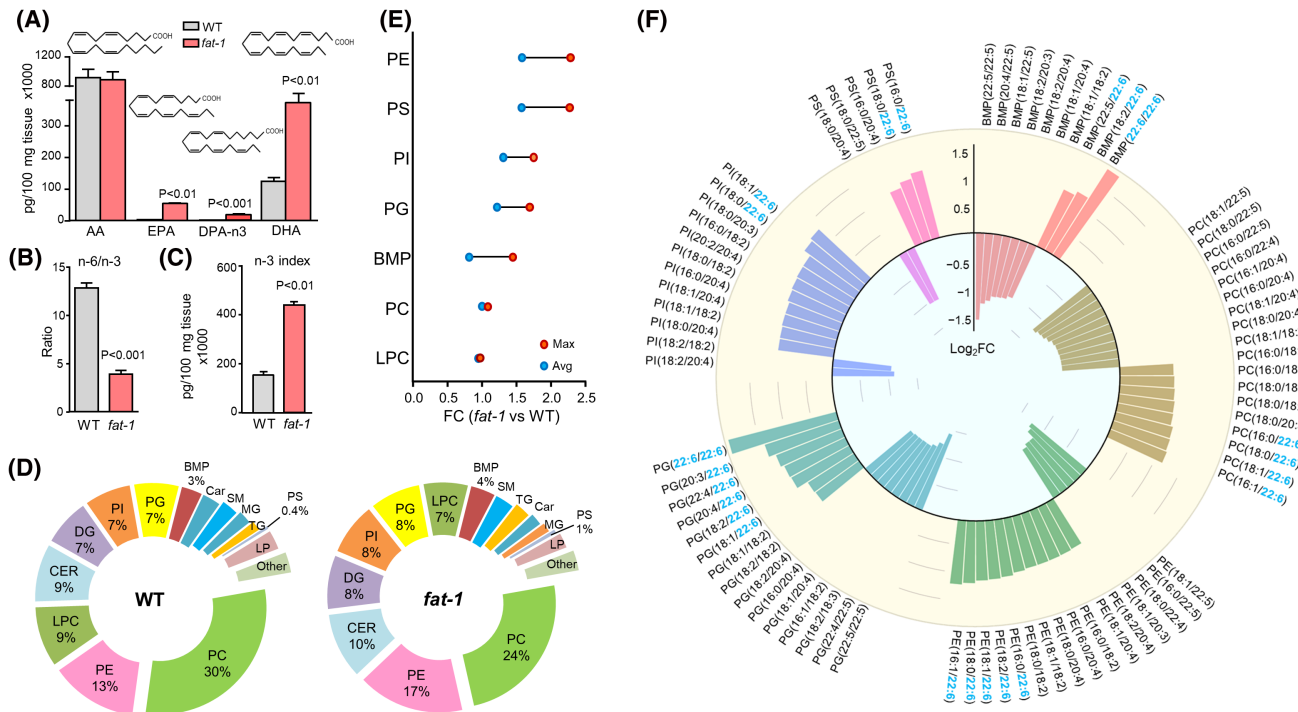
FIGURE 3 Targeted and untargeted liquid chromatography–tandem mass spectrometry (LC–MS/MS) analyses identify a specific lipidome signature in omega-3 polyunsaturated fatty acid (PUFA)–enriched tissues. (A) Targeted LC–MS/MS analysis of arachidonic acid (AA), eicosapentaenoic acid (EPA), docosapentaenoic acid omega-3 (DPA n-3), and docosahexaenoic acid (DHA) levels in the liver from wild-type (WT) ($n = 3$) and *fat-1* ($n = 3$) mice. (B) Liver omega-6 (n-6)– to omega-3 (n-3)–PUFAs ratio. (C) n-3 index as calculated by the total amount of EPA and DHA. (D) Pie charts of liver lipid class distribution in WT ($n = 3$) and *fat-1* ($n = 3$) mice as assessed by untargeted LC–MS/MS analysis. (E) Lollipop charts of total content of phospholipid subclasses. (F) Circos plot of the fold changes between *fat-1* and WT mice for each individual phospholipid. The presence of DHA (C22:6) is highlighted in blue. Lipid values were log2 transformed before calculating the fold changes between *fat-1* and WT mice. BMP, bis(monoacylglycero)phosphate; Car, acyl carnitine; CER, ceramide; DG, diglyceride; FC, fold change; LP, lysophosphatidylethanolamine; LPC, lysophosphatidylcholine; MG, monoglyceride; PC, phosphatidylcholine; PE, phosphatidylethanolamine; PG, phosphatidylglycerol; PI, phosphatidylinositol; PS, phosphatidylserine; SM, sphingomyelin; TG, triglyceride.

assessed the profile of the biosynthetic intermediates of these lipid autacoids derived from DHA and EPA by targeted LC–MS/MS analysis in livers from *fat-1* and WT mice. As compared with WT, *fat-1* mice showed higher hepatic levels of the small lipid autacoid markers/intermediates 14–hydroxy-DHA (HDHA), 17-HDHA, and 18–hydroxy-EPA (Figure 5A). We then assessed the profile of bioactive lipid autacoids and identified that DHA-derived lipid autacoids, namely resolvin D1 (RvD1) and 7(R)–maresin 1 (MaR1) were the most abundant in *fat-1* mice (Figure 5B). In fact, both RvD1 and MaR1 were increased in *fat-1* with respect to WT mice (Figure 5C). Conversely, tissue levels of AA-derived products (i.e., prostaglandin E_2, leukotriene E_4, prostaglandin D_2, thromboxane B_2, prostaglandin $F_{2\alpha}$, and 6-keto–prostaglandin $F_{1\alpha}$) were lower in *fat-1* than WT mice (Figure 5B). To test the metabolic effectiveness of RvD1 and MaR1, we incubated hepatocytes with these lipid autacoids and performed metabolic flux analysis after exposure to TNFα, a cytotoxic cytokine that induces mitochondrial damage.[30,31] As shown in Figure 5D–F, hepatocytes incubated for 6 h with TNFα displayed

reduced metabolic rates for TCA cycle substrates and intermediates (isocitrate, glutamate, fumarate, malate, pyruvate, *cis*-aconitate, and succinate), long-chain acyl-carnitines (palmitoyl-*D*,L-carnitine and octanoyl-L-carnitine), and amino acids D-glucose-1-P and glycogen. In this model, RvD1 and MaR1 prevented the damaging actions of TNFα on hepatocyte utilization of TCA cycle substrates and intermediates (Figure 5G). The protective effect of RvD1 and MaR1 against TNFα-induced metabolic derangement can be visualized in a radar chart in Figure 5H. RvD1 and MaR1 also counterregulated TNFα-induced impairment of metabolic rates for acyl-carnitines (Figure 5I) and carbohydrates (Figure 5J). The protective actions of RvD1 and MaR1 were not observed when hepatocytes were incubated with TNFα for shorter periods of time (1 h) (Figure S4). Finally, we tested whether the metabolic effects of DHA-derived lipid autacoids could be reproduced by the intermediate precursor 17-HDHA. 17-HDHA was only efficacious in inducing changes of the metabolic rate under resting conditions but not under TNFα stimulation (Figure S5A,B).
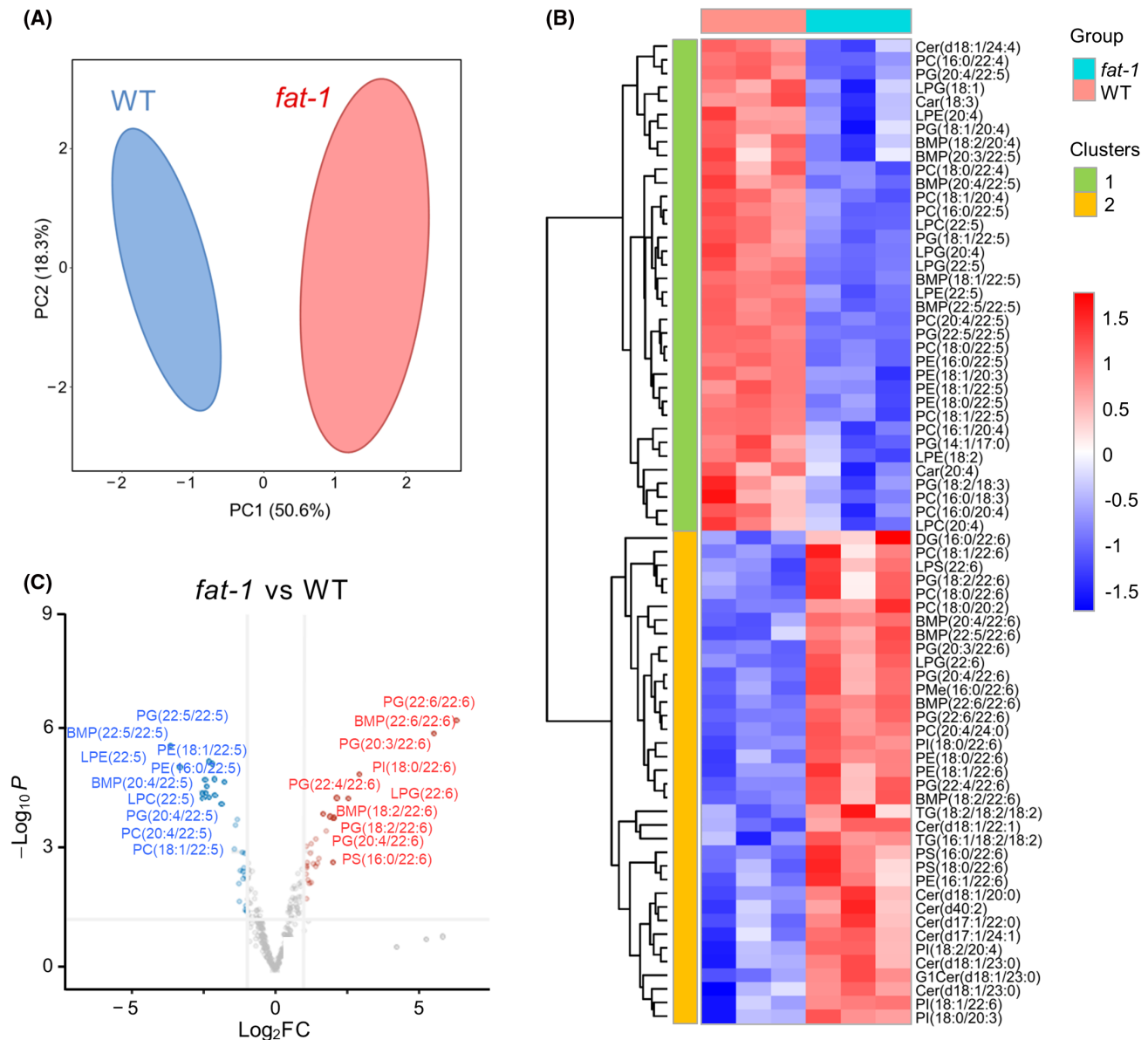
FIGURE 4 Distinct composition of phospholipid subclasses containing the omega-3–polyunsaturated fatty acid docosahexaenoic acid. (A) Principal component analysis. (B) Heatmap of individual lipid species ranked by fold change (red, up-regulated; blue, down-regulated) and significant false discovery rate changes between *fat-1* (*n* = 3) and wild-type (WT) (*n* = 3) mice. (C) Volcano plot representing the levels of lipid species with the highest positive significant changes (red) and the highest negative significant changes (blue) between *fat-1* and WT mice. BMP, bis(monoacylglycero)phosphate; Car, acyl carnitine; Cer, ceramide; FC, fold change; LPE, lysophosphatidylethanolamine; LPG, lysophosphatidylglycerol; PC, phosphatidylcholine; PE, phosphatidylethanolamine; PG, phosphatidylglycerol; PI, phosphatidylinositol; PMe, phosphatidylmethylethanolamine; PS, phosphatidylserine; TG, triglyceride.

Fat-1 mice are protected from the obesogenic effects of HFD feeding

Because mitochondria play a central role in metabolism and energy expenditure,[32] we next investigated the response of *fat-1* mice to HFD-induced obesity. The design of these experiments is shown in Figure S6A. After prolonged (24 weeks) HFD feeding, the mice became obese in comparison with mice receiving chow diet, although *fat-1* mice gained significantly less body weight than WT mice (Figure 6A). No differences in food intake were seen between *fat-1* and WT mice (Figure S6B),

but reduced body weight gain in *fat-1* mice was associated with lower eWAT (Figure S6C). No changes in iBAT mass were observed, although the weight ratio between iBAT, which is rich in mitochondria, and eWAT under chow conditions was significantly higher in *fat-1* in comparison with WT mice (Figure S6D,E). The expression of markers of thermogenesis was also increased in iBAT from *fat-1* mice, under both chow (Figure S6F) and HFD (Figure S6G). Furthermore, *fat-1* mice showed a more intense eWAT browning than WT mice (Figure S6H). Taken together, these findings support the view that *fat-1* mice have a superior metabolic profile.
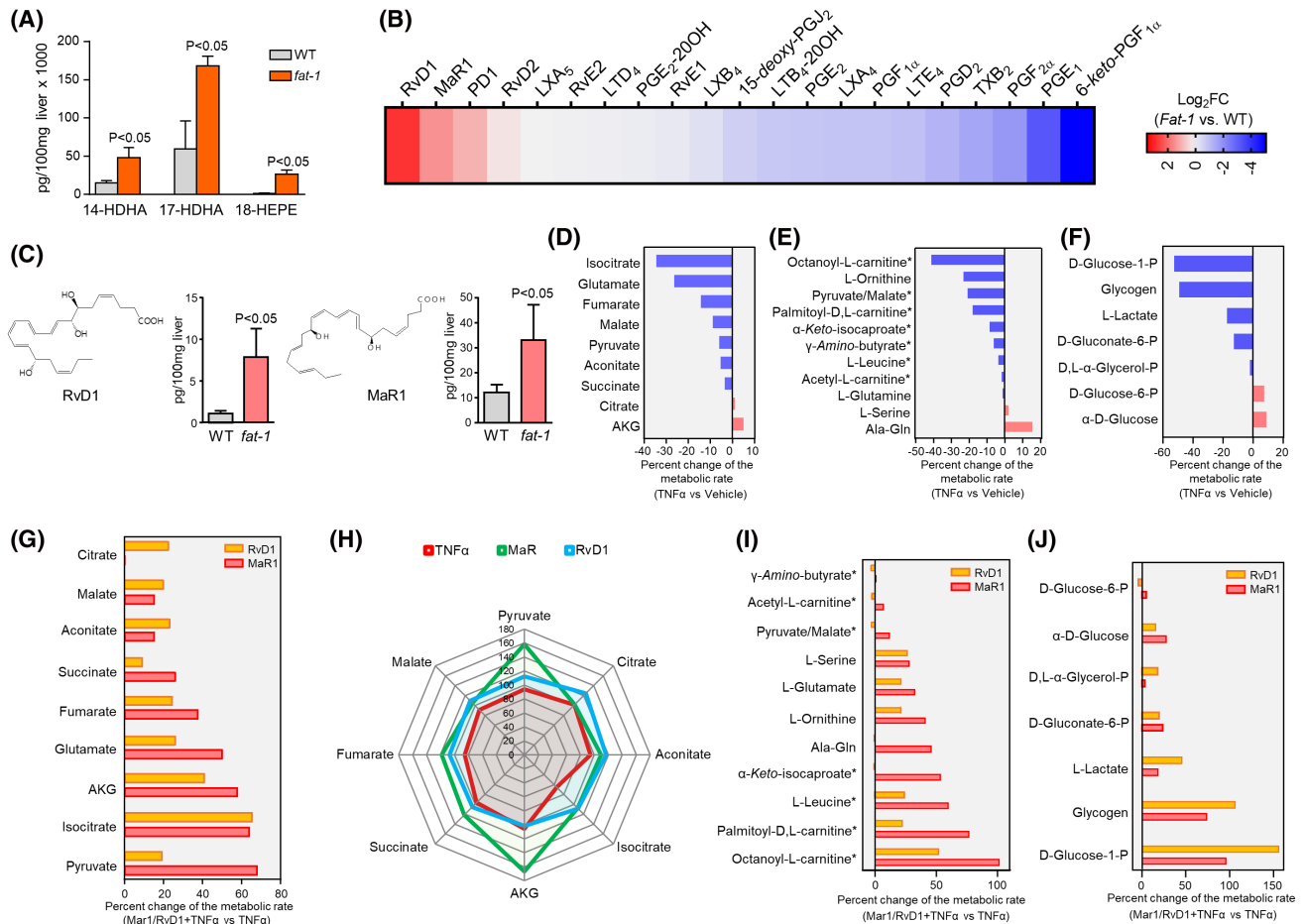
FIGURE 5 Small lipid autacoids derived from docosahexaenoic acid protect hepatocytes from TNFα-induced mitochondrial injury. (A) Targeted liquid chromatography–tandem mass spectrometry (LC–MS/MS) analysis of the biosynthetic intermediates 14-hydroxy–docosahexaenoic acid (HDHA), 17-HDHA, and 18–hydroxy-eicosapentaenoic acid (HEPE) levels in livers of wild-type (WT) ($n = 3$) and *fat-1* ($n = 3$) mice. (B) Ranking of fold changes in the levels of lipid autacoids between *fat-1* and WT mice. (C) Targeted LC–MS/MS analysis of resolvin D1 (RvD1) and maresin 1 (MaR1) in livers from WT ($n = 3$) and *fat-1* ($n = 3$) mice. (D) Bar plots representing the percent changes of the metabolic rate for tricarboxylic acid (TCA) cycle substrates and intermediates in WT primary hepatocytes ($n = 5$) incubated for 6h with either vehicle (0.1% BSA) or TNFα (20ng/mL) in the absence of actinomycin D. (E) The same as in (D) but for fatty acid and amino acid substrates. (F) As in (D) and (E) but for carbohydrate substrates. (G) Percent changes of the metabolic rate for TCA cycle substrates and intermediates in primary hepatocytes from WT mice ($n = 5$) pretreated with either vehicle (0.03% ethanol), MaR1 (10nM) or RvD1 (10nM) for 1h and stimulated with TNFα (20ng/mL) for 6h. (H) Radar chart representing TCA cycle substrates and utilization of intermediates. (I) Percent changes of the metabolic rate for fatty acid and amino acid substrates. (J) Percent changes of the metabolic rate for carbohydrate substrates. Malate was added to these substrates at a concentration of 100μM. 20-OH, 20-hydroxy; AKG, α-*keto*-glutarate; Ala-Gln, alanyl-glutamine; BSA, bovine serum albumin; FC, fold change; LTB_4, leukotriene B_4; LTD_4, leukotriene D_4; LTE_4, leukotrine E_4; LXA_5, lipoxin A_5; LXB_4, lipoxin B_4; PD1, protectin D1; PGD_2, prostaglandin D_2; PGE, prostaglandin E; PGF, prostaglandin F; PGJ_2, prostaglandin J_2; RvE, resolvin E; TXB_2, thromboxane B_2.

Fat-1 mice are protected from HFD-induced metabolic dysfunction

We next investigated the liver phenotype of *fat-1* mice subjected to the HFD-induced obesity model. After 24 weeks of HFD feeding, oil red-O staining of liver sections revealed widespread steatosis in WT, but not in *fat-1* mice (Figure 6B). The observation that *fat-1* mice were resistant to HFD-induced hepatic steatosis was confirmed by quantifying the total area stained by oil red-O and the tissue TAG levels (Figure 6C). Furthermore, H&E staining of liver sections showed higher liver injury in WT than in *fat-1* mice (Figure 6D and Figure S7A). In addition, as compared with WT,

fat-1 mice showed higher hepatic AKT phosphorylation and TIM44 levels (Figure 6E,F). Although HFD feeding reduced coupling OXPHOS and maximal respiration in WT (Figure 6G inset) and *fat-1* (Figure S7B) mice, *fat-1* still retained higher respiration capacity and mitochondrial FAO than WT mice (Figure 6H,I and Figure S1B).

Fat-1 mice are protected from liver injury induced by the CDAHFD fibrogenic diet

We finally tested the response of *fat-1* mice to CDAHFD, which models fatty liver disease at more advanced stages when liver injury is characterized
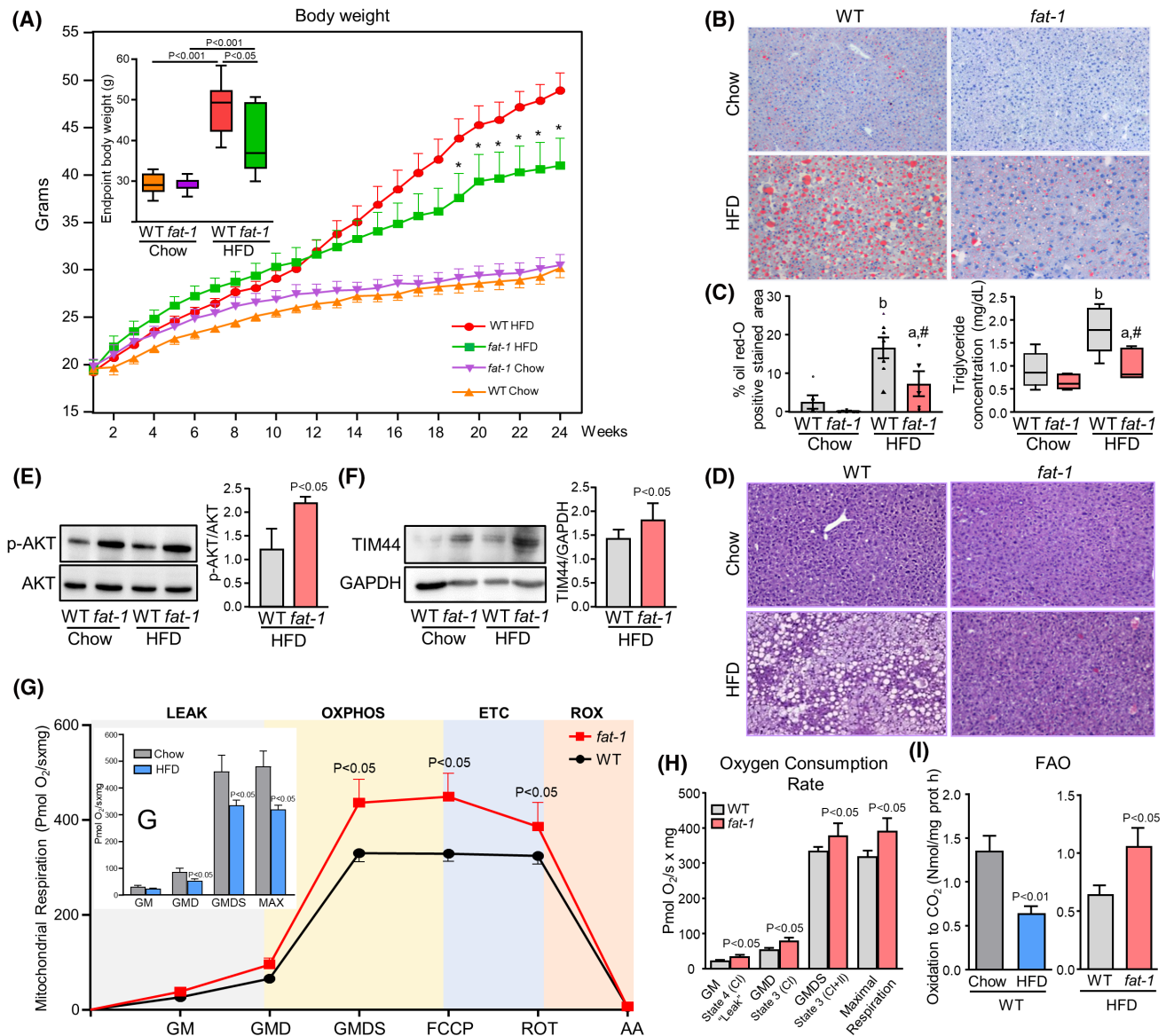
FIGURE 6 *Fat-1* mice are protected against mitochondrial dysfunction induced by a steatogenic diet. (A) Weekly body weight values of wild-type (WT) ($n = 24$) and *fat-1* ($n = 18$) mice receiving either a chow diet or high-fat diet (HFD) for 24 weeks. Endpoint body weights are shown in the inset. (B) Representative photomicrographs at 100× magnification of liver sections stained with oil red-O. (C) Percentage of the area stained with oil red-O and hepatic triglyceride concentration. (D) Representative photomicrographs at 100× magnification of liver sections stained with hematoxylin and eosin. (E) Phosphorylated serine/threonine protein kinase (p-AKT) and total serine/threonine protein kinase (AKT) protein expression in livers from WT and *fat-1* mice receiving HFD. The ratio between p-AKT and AKT is shown on the right. (F) Translocase of inner mitochondrial membrane 44 protein expression in the experiments described in (E). (G) Oxygen consumption rate (OCR) of isolated mitochondria from livers of WT and *fat-1* mice receiving HFD as measured by high-resolution respirometry using substrate/inhibitor titration protocol. Inset: OCR values of isolated mitochondria from livers of WT mice receiving either chow diet or HFD. (H) OCR corrected for ROX in mice receiving either chow diet or HFD. (I) Measurements of radiolabeled [1-^{14}C] oleate β-oxidation (FAO) of isolated mitochondria from livers of the animals of the study receiving either chow diet or HFD. a, $p < 0.05$ versus chow; b, $p < 0.01$ versus chow; #, $p < 0.01$ versus HFD. AA, arachidonic acid; CI, complex I; CII, complex II; ETC, electron transport chain; FCCP, carbonylcyanide-4-(trifluoromethoxy)-phenylhydrazone; GM, glutamate/malate; GMD, GM/adenosine diphosphate; GMDS, GMD/succinate; MAX, maximal respiration; OXPHOS, oxidative phosphorylation; ROT, rotenone; ROX, residual oxygen consumption.

by extensive liver fibrosis. The experimental design is shown in Figure S7C. Similar to the HFD model, *fat-1* mice had higher iBAT and iBAT/eWAT weight ratios after 24 weeks of CDAHFD feeding than WT mice (Figure S7D). Importantly, the extension of liver fibrosis was lower in *fat-1* than in WT mice (Figure 7A,B). No differences in response to CDAHFD were seen in the

levels of AST ALT and TAG and in the expression of MCP-1 and TNFα between *fat-1* and WT mice, likely reflecting the very advanced stages of liver injury in this model (Figure 7E,F). At the end of the 24 weeks of CDAHFD treatment, *fat-1* mice showed higher insulin sensitivity (AKT phosphorylation) (Figure 7C) but similar content of TIM44 (Figure 7D). CDAHFD feeding
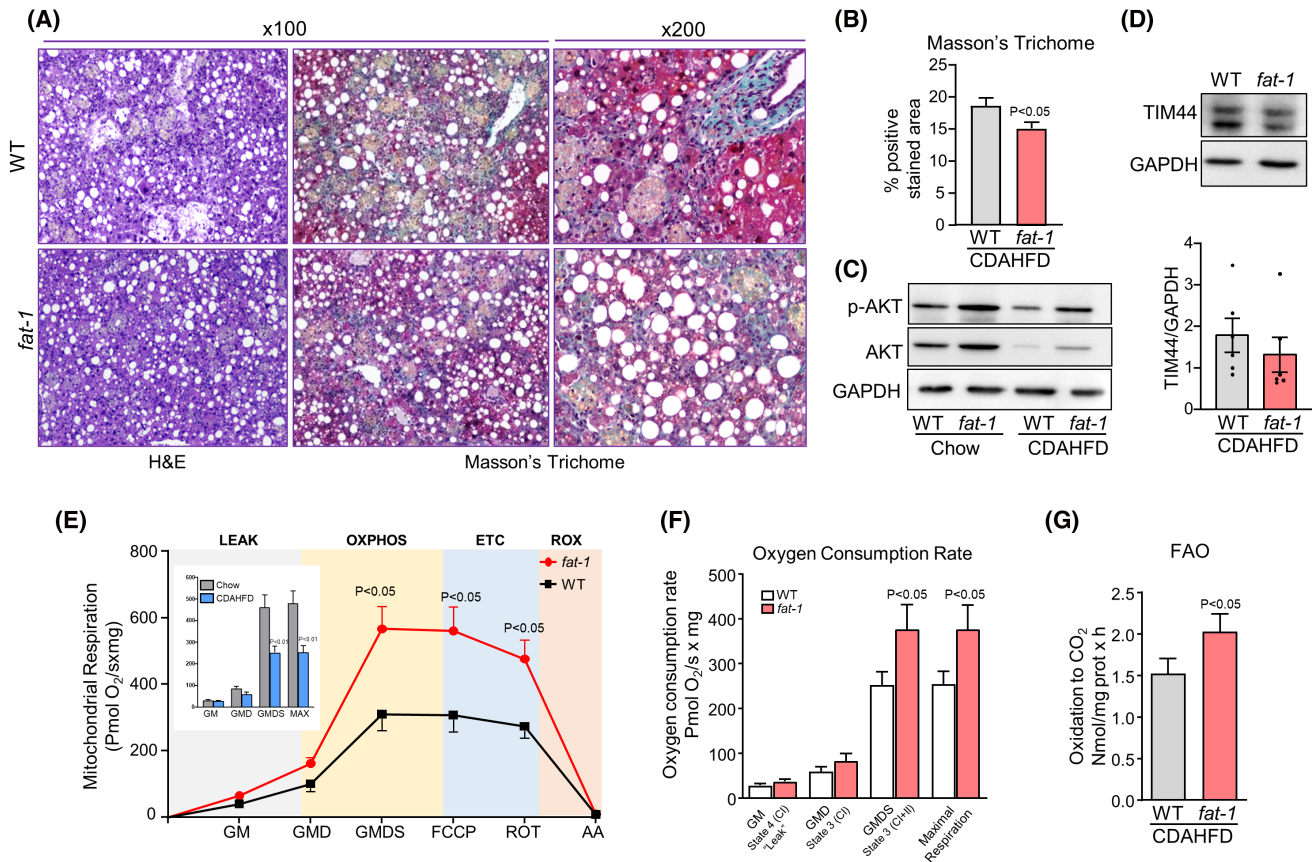
FIGURE 7 *Fat-1* mice are protected against mitochondrial dysfunction induced by a fibrogenic diet. (A) Representative photomicrographs at 100× and 200× magnification of liver sections stained with hematoxylin and eosin (H&E) and Masson's trichrome from wild-type (WT) (*n* = 10) and *fat-1* (*n* = 8) mice receiving a fibrogenic choline-deficient L-amino acid–defined diet in combination with HFD (CDAHFD) for 24 weeks. (B) Histomorphometric analysis of the area stained with Masson's trichrome. (C) Phosphorylated serine/threonine protein kinase (p-AKT) and total serine/threonine protein kinase (AKT) hepatic protein expression. (D) Representative blots of translocase of inner mitochondrial membrane 44 (TIM44) protein expression. The densitometry of TIM44 signal normalized to glyceraldehyde 3-phosphate dehydrogenase (GAPDH) is shown below. (E) Oxygen consumption rate (OCR) of isolated mitochondria from livers of WT and *fat-1* mice receiving CDAHFD as measured by high-resolution respirometry using the substrate/inhibitor titration protocol. Inset: OCR values of isolated mitochondria from livers of WT mice receiving either chow diet or CDAHFD. (F) OCR values corrected for ROX in mice receiving CDAHFD. (G) Measurements of radiolabeled [1-^{14}C] oleate β-oxidation (FAO) of mitochondria isolated from livers of the study animals receiving CDAHFD. CI, complex I; CII, complex II; FCCP, carbonylcyanide-4-(trifluoromethoxy)-phenylhydrazone; GM, glutamate/malate; GMD, GM/adenosine diphosphate; GMDS, GMD/succinate; MAX, maximal respiration; OXPHOS, oxidative phosphorylation; ROT, rotenone; ROX, residual oxygen consumption.

impaired coupling OXPHOS and maximal respiration in both WT (Figure 7E inset) and *fat-1* (Figure S7G) mice, although *fat-1* again displayed higher respiration capacity and FAO than WT mice (Figure 7E–G and Figure S1C).

DISCUSSION

The results of the current study provide evidence that tissue enrichment with omega-3−PUFAs is beneficial in terms of metabolic fitness. Our study was performed in *fat-1* mice, a transgenic animal model in which tissues are endogenously enriched with omega-3−PUFAs[17,33] to avoid any confounding factor related to diet. In these mice, we demonstrated that enrichment with omega-3−PUFAs is associated with more optimal liver mitochondrial function, particularly a higher mitochondrial content and capacity and superior mitochondrial respiration and FAO. In addition, *fat-1* mice showed improved mitochondrial fission/fusion balance and mitochondrial dynamics. Furthermore, *fat-1* mice exhibited increased levels of TIM44, a housekeeping membrane transport protein that facilitates the process of protein import from the inner membrane into the mitochondrial matrix in an ATP-dependent manner, leading to increased mitochondrial ATP production.[26,34]

The lipid composition of mitochondria is mostly dominated by PC and PE, which account for 80% of total phospholipids. Mitochondria also contain 10%–15% of cardiolipin (diphosphatidylglycerol) and a marginal

content in sphingolipids.[6] Moreover, mitochondria are endowed with enzymes involved in lipid synthesis, and this organelle actively contributes to the biosynthesis of phospholipids from phosphatidic acid (Figure S2).[6] Notably, the outer and inner mitochondrial membranes are highly specialized and differ in lipid composition for optimal membrane and enzyme function.[6,35] Specifically, the outer membrane is rich in lipids to maintain its high fluidity, whereas the inner is characterized by low lipid and high protein content.[6] Because of their chain length and multiple double bonds, the incorporation of omega-3−PUFAs into mitochondrial membranes alters the viscosity of the lipid bilayer (membrane fluidity), thus modulating lipid−lipid and lipid−protein interactions.[35] Although the design of the current study did not allow us to discern at which level changes in lipid composition in *fat-1* mice impact mitochondrial function, several lines of evidence suggest that omega-3 enrichment could be related to changes in the inner mitochondrial membrane. For instance, our observation that *fat-1* mice had superior OXPHOS activity and higher protein content of complexes I and II might be the result of changes in the lipid composition of the inner membrane leading to changes in the organization and dynamics of cristae, which contain the protein complexes responsible for OXPHOS.[36] In fact, previous studies have reported that PUFA-deficient rats develop dramatic impairment in OXPHOS, whereas omega-3−PUFA enrichment translates into enhanced ADP kinetics,[37,38] suggesting that a higher omega-3−PUFA content would mainly impact inner membrane lipid composition. Consistent with this, increased levels of omega-3−PUFAs in the inner mitochondrial membrane are associated with lower proton leak rates.[39] Moreover, within the phospholipid class, *fat-1* mice mainly differed from WT by increased PE content, which is characteristically more abundant in the inner than in the outer mitochondrial membrane.[36] Collectively, our findings indicate that endogenous omega-3−PUFA enrichment promotes the reorganization of the membrane lipid composition, impacting not only its fluidity but also the function of cell organelles such as mitochondria.

The results of the current study provide evidence that omega-3−PUFAs might affect mitochondrial integrity and function independently of changes in membrane lipid composition. In fact, our experiments in hepatocytes provide evidence that lipid autacoids from DHA, namely RvD1 and MaR1, protect these cells against TNFα-induced mitochondrial injury in the absence of transcriptional arrest. Particularly, RvD1 and MaR1 prevented the damaging actions of TNFα on hepatocyte utilization of TCA cycle substrates and intermediates. These findings are consistent with other studies showing that RvD1 reduces mitochondrial swelling and restores mitochondrial respiratory activity and mitochondrial biogenesis in liver cells and protects mitochondrial membrane potential in astrocytes.[14,15]

Resolvin E1, which is an EPA-derived lipid autacoid, also improves mitochondrial function in alveolar epithelial cells and restores TNFα-induced inflammatory mitochondrial dysfunction.[16,26] Together, these findings reinforce the beneficial role of essential omega-3−PUFA-derived lipid autacoids in protecting mitochondria from inflammatory injury.

The results of the current study also provide a mechanistic basis by which *fat-1* mice are resistant to obesity-induced hepatic steatosis, insulin resistance, inflammation in insulin-sensitive tissues (white adipose tissue [WAT] and liver), and liver fibrosis.[18,19] Our findings might also explain why animals endogenously enriched with omega-3−PUFAs are protected against alcohol-induced liver injury,[40] a condition characterized by widespread mitochondrial damage.[41] Our study also provides some mechanistic insights beyond the liver cells as to why omega-3−PUFA-enriched animals have a reduced risk for noncommunicable diseases including metabolic disease, colon inflammation-triggered injury, pancreatitis, acute lung injury, inflammatory burden during preterm birth, vascular inflammation, and neuroinflammatory injury among others in which loss of mitochondria function is common.[20,21,32,42−46]

Our data might have translation to the clinic. Previous studies have demonstrated a lower content of omega-3−PUFAs in the liver of patients with NAFLD[18] as well as a reduced content of omega-3−derived lipid autacoids in the circulation and the WAT of obese individuals.[47,48] Importantly, in patients with NASH, 15−18-month treatment with DHA plus EPA produced decreased liver fat content, whereas the administration of an omega-3−rich diet for 6 months resulted in improved hepatic mitochondrial function.[49,50] Finally, administration of highly purified EPA showed biopsy-proven improvement of hepatic steatosis, fibrosis, hepatocyte ballooning, and lobular inflammation,[51] although EPA in its ethyl form failed to exert any significant effect on liver histology despite reducing TAG levels compared with placebo.[52]

In summary, our study highlights the critical role of having a tissue environment enriched in omega-3−PUFA to preserve and enhance mitochondrial efficiency in liver cells. Our data also unveil the ability of omega-3−PUFA derivatives to protect liver mitochondria from inflammatory injury. This finding adds further value to the well-established antiinflammatory and proresolving properties of these bioactive lipid mediators to counteract the damaging actions of unresolved inflammation. Because mitochondria are central organelles to the pathogenesis of metabolic dysfunction, our study underscores the critical role of maintaining healthy nutritional support with essential FAs during the clinical management of this disease.

AUTHOR CONTRIBUTIONS

Cristina López-Vicario and Joan Clària conceived and designed the experiments; Cristina López-Vicario,

CONFLICT OF INTEREST
Nothing to report.

DATA AVAILABILITY STATEMENT
The authors confirm that the data supporting the findings of this study are available within the article and the online Supporting Information.

ORCID
Cristina López-Vicario https://orcid.org/0000-0002-6609-8501
Mireia Casulleras https://orcid.org/0000-0002-2899-5826
Marta Duran-Güell https://orcid.org/0000-0002-3265-395X
Roger Flores-Costa https://orcid.org/0000-0002-8711-2552
Ingrid W. Zhang https://orcid.org/0000-0001-6328-8257
Esther Titos https://orcid.org/0000-0002-2543-2243
Joan Clària https://orcid.org/0000-0003-4333-7749

REFERENCES
1. Scheibye-Knudsen M, Fang EF, Croteau DL, Wilson DM 3rd, Bohr VA. Protecting the mitochondrial powerhouse. Trends Cell Biol. 2015;25(3):158–70.
2. McLaughlin KL, Hagen JT, Coalson HS, Nelson MAM, Kew KA, Wooten AR, et al. Novel approach to quantify mitochondrial content and intrinsic bioenergetic efficiency across organs. Sci Rep. 2020;10(1):17599.
3. Samuel VT, Shulman GI. Nonalcoholic fatty liver disease as a nexus of metabolic and hepatic diseases. Cell Metab. 2018;27(1):22–41.
4. Mansouri A, Gattolliat CH, Asselah T. Mitochondrial dysfunction and signaling in chronic liver diseases. Gastroenterology. 2018;155(3):629–47.
5. Schuster S, Cabrera D, Arrese M, Feldstein AE. Triggering and resolution of inflammation in NASH. Nat Rev Gastroenterol Hepatol. 2018;15(6):349–64.
6. Horvath SE, Daum G. Lipids of mitochondria. Prog Lipid Res. 2013;52(4):590–614.
7. Monteiro JP, Oliveira PJ, Jurado AS. Mitochondrial membrane lipid remodeling in pathophysiology: a new target for diet and therapeutic interventions. Prog Lipid Res. 2013;52(4):513–28.
8. Cocco T, Di Paola M, Papa S, Lorusso M. Arachidonic acid interaction with the mitochondrial electron transport chain promotes reactive oxygen species generation. Free Radic Biol Med. 1999;27(1–2):51–9.
9. Scorrano L, Penzo D, Petronilli V, Pagano F, Bernardi P. Arachidonic acid causes cell death through the mitochondrial permeability transition. Implications for tumor necrosis factor-alpha apoptotic signaling. J Biol Chem. 2001;276(15):12035–40.
10. O'Connell KA, Dabkowski ER, de Fatima GT, Xu W, Daneault C, de Rosiers C, et al. Dietary saturated fat and docosahexaenoic acid differentially effect cardiac mitochondrial phospholipid fatty acyl composition and Ca(2+) uptake, without altering permeability transition or left ventricular function. Physiol Rep. 2013;1(1):e00009.
11. Pepe S, Tsuchiya N, Lakatta EG, Hansford RG. PUFA and aging modulate cardiac mitochondrial membrane lipid composition and Ca2+ activation of PDH. Am J Physiol. 1999;276(1):H149–58.
12. Zhang Y, Jiang L, Hu W, Zheng Q, Xiang W. Mitochondrial dysfunction during in vitro hepatocyte steatosis is reversed by omega-3 fatty acid-induced up-regulation of mitofusin 2. Metabolism. 2011;60(6):767–75.
13. Johnson ML, Lalia AZ, Dasari S, Pallauf M, Fitch M, Hellerstein MK, et al. Eicosapentaenoic acid but not docosahexaenoic acid restores skeletal muscle mitochondrial oxidative capacity in old mice. Aging Cell. 2015;14(5):734–43.
14. Kang JW, Choi HS, Lee SM. Resolvin D1 attenuates liver ischaemia/reperfusion injury through modulating thioredoxin 2-mediated mitochondrial quality control. Br J Pharmacol. 2018;175(12):2441–53.
15. Ren YZ, Zhang BZ, Zhao XJ, Zhang ZY. Resolvin D1 ameliorates cognitive impairment following traumatic brain injury via protecting astrocytic mitochondria. J Neurochem. 2020;154(5):530–46.
16. Mayer K, Sommer N, Hache K, Hecker A, Reiche S, Schneck E, et al. Resolvin E1 improves mitochondrial function in human alveolar epithelial cells during severe inflammation. Lipids. 2019;54(1):53–65.
17. Kang JX, Wang J, Wu L, Kang ZB. Transgenic mice: fat-1 mice convert n-6 to n-3 fatty acids. Nature. 2004;427(6974):504.

18. López-Vicario C, González-Périz A, Rius B, Morán-Salvador E, García-Alonso V, Lozano JJ, et al. Molecular interplay between Δ5/Δ6 desaturases and long-chain fatty acids in the pathogenesis of non-alcoholic steatohepatitis. Gut. 2014;63(2):344–55.

19. López-Vicario C, Alcaraz-Quiles J, García-Alonso V, Rius B, Hwang SH, Titos E, et al. Inhibition of soluble epoxide hydrolase modulates inflammation and autophagy in obese adipose tissue and liver: role for omega-3 epoxides. Proc Natl Acad Sci U S A. 2015;112(2):536–41.

20. White PJ, Arita M, Taguchi R, Kang JX, Marette A. Transgenic restoration of long-chain n-3 fatty acids in insulin target tissues improves resolution capacity and alleviates obesity-linked inflammation and insulin resistance in high-fat-fed mice. Diabetes. 2010;59(12):3066–73.

21. Hudert CA, Weylandt KH, Lu Y, Wang J, Hong S, Dignass A, et al. Transgenic mice rich in endogenous omega-3 fatty acids are protected from colitis. Proc Natl Acad Sci U S A. 2006;103(30):11276–81.

22. Wigglesworth VB. The use of osmium in the fixation and staining of tissues. Proc R Soc Lond B Biol Sci. 1957;147(927): 185–99.

23. Tsugawa H, Ikeda K, Takahashi M, Satoh A, Mori Y, Uchino H, et al. A lipidome atlas in MS-DIAL 4. Nat Biotechnol. 2020;38(10):1159–63.

24. Naoe S, Tsugawa H, Takahashi M, Ikeda K, Arita M. Characterization of lipid profiles after dietary intake of polyunsaturated fatty acids using integrated untargeted and targeted lipidomics. Metabolites. 2019;9(10):241.

25. Galloway CA, Lee H, Brookes PS, Yoon Y. Decreasing mitochondrial fission alleviates hepatic steatosis in a murine model of nonalcoholic fatty liver disease. Am J Physiol Gastrointest Liver Physiol. 2014;307(6):G632–41.

26. Hecker M, Sommer N, Foch S, Hecker A, Hackstein H, Witzenrath M, et al. Resolvin E1 and its precursor 18R-HEPE restore mitochondrial function in inflammation. Biochim Biophys Acta Mol Cell Biol Lipids. 2018;1863(9):1016–28.

27. Li W, Cheng H, Li G, Zhang L. Mitochondrial damage and the road to exhaustion. Cell Metab. 2020;32(6):905–7.

28. Hullin-Matsuda F, Luquain-Costaz C, Bouvier J, Delton-Vandenbroucke I. Bis(monoacylglycero)phosphate, a peculiar phospholipid to control the fate of cholesterol: Implications in pathology. Prostaglandins Leukot Essent Fatty Acids. 2009;81(5–6):313–24.

29. Serhan CN. Pro-resolving lipid mediators are leads for resolution physiology. Nature. 2014;510(7503):92–101.

30. Schulze-Osthoff K, Bakker AC, Vanhaesebroeck B, Beyaert R, Jacob WA, Fiers W. Cytotoxic activity of tumor necrosis factor is mediated by early damage of mitochondrial functions. Evidence for the involvement of mitochondrial radical generation. J Biol Chem. 1992;267(8):5317–23.

31. Kastl L, Sauer SW, Ruppert T, Beissbarth T, Becker MS, Süss D, et al. TNF-α mediates mitochondrial uncoupling and enhances ROS-dependent cell migration via NF-κB activation in liver cells. FEBS Lett. 2014;588(1):175–83.

32. Liesa M, Shirihai OS. Mitochondrial dynamics in the regulation of nutrient utilization and energy expenditure. Cell Metab. 2013;17(4):491–506.

33. Kaliannan K, Li XY, Wang B, Pan Q, Chen CY, Hao L, et al. Multi-omic analysis in transgenic mice implicates omega-6/omega-3 fatty acid imbalance as a risk factor for chronic disease. Commun Biol. 2019;2:276.

34. Matsuoka T, Wada J, Hashimoto I, Zhang Y, Eguchi J, Ogawa N, et al. Gene delivery of Tim44 reduces mitochondrial superoxide production and ameliorates neointimal proliferation of injured carotid artery in diabetic rats. Diabetes. 2005;54(10):2882–90.

35. Sullivan EM, Pennington ER, Green WD, Beck MA, Brown DA, Shaikh SR. Mechanisms by which dietary fatty acids regulate mitochondrial structure-function in health and disease. Adv Nutr. 2018;9(3):247–62.

36. Joubert F, Puff N. Mitochondrial cristae architecture and functions: lessons from minimal model systems. Membranes (Basel). 2021;11(7):465.

37. Fontaine EM, Moussa M, Devin A, Garcia J, Ghisolfi J, Rigoulet M, et al. Effect of polyunsaturated fatty acids deficiency on oxidative phosphorylation in rat liver mitochondria. Biochim Biophys Acta. 1996;1276(3):181–7.

38. Herbst EA, Paglialunga S, Gerling C, Whitfield J, Mukai K, Chabowski A, et al. Omega-3 supplementation alters mitochondrial membrane composition and respiration kinetics in human skeletal muscle. J Physiol. 2014;592(6):1341–52.

39. Pehowich DJ. Thyroid hormone status and membrane n-3 fatty acid content influence mitochondrial proton leak. Biochim Biophys Acta. 1999;1411(1):192–200.

40. Warner J, Hardesty J, Song Y, Sun R, Deng Z, Xu R, et al. Fat-1 transgenic mice with augmented n3-polyunsaturated fatty acids are protected from liver injury caused by acute-on-chronic ethanol administration. Front Pharmacol. 2021;12:711590.

41. Hoek JB, Cahill A, Pastorino JG. Alcohol and mitochondria: a dysfunctional relationship. Gastroenterology. 2002;122(7):2049–63.

42. Yamashita A, Kawana K, Tomio K, Taguchi A, Isobe Y, Iwamoto R, et al. Increased tissue levels of omega-3 polyunsaturated fatty acids prevents pathological preterm birth. Sci Rep. 2013;3:3113.

43. Weylandt KH, Nadolny A, Kahlke L, Köhnke T, Schmöcker C, Wang J, et al. Reduction of inflammation and chronic tissue damage by omega-3 fatty acids in fat-1 transgenic mice with pancreatitis. Biochim Biophys Acta. 2008;1782(11):634–41.

44. Mayer K, Kiessling A, Ott J, Schaefer MB, Hecker M, Henneke I, et al. Acute lung injury is reduced in fat-1 mice endogenously synthesizing n-3 fatty acids. Am J Respir Crit Care Med. 2009;179(6):474–83.

45. Wan JB, Huang LL, Rong R, Tan R, Wang J, Kang JX. Endogenously decreasing tissue n-6/n-3 fatty acid ratio reduces atherosclerotic lesions in apolipoprotein E-deficient mice by inhibiting systemic and vascular inflammation. Arterioscler Thromb Vasc Biol. 2010;30(12):2487–94.

46. Hopperton KE, Trépanier MO, Giuliano V, Bazinet RP. Brain omega-3 polyunsaturated fatty acids modulate microglia cell number and morphology in response to intracerebroventricular amyloid-β1-40 in mice. J Neuroinflammation. 2016;13(1):257.

47. Titos E, Rius B, López-Vicario C, Alcaraz-Quiles J, García-Alonso V, Lopategi A, et al. Signaling and immunoresolving actions of resolvin D1 in inflamed human visceral adipose tissue. J Immunol. 2016;197(8):3360–70.

48. López-Vicario C, Titos E, Walker ME, Alcaraz-Quiles J, Casulleras M, Durán-Güell M, et al. Leukocytes from obese individuals exhibit an impaired SPM signature. FASEB J. 2019;33(6):7072–83.

49. Scorletti E, Bhatia L, McCormick KG, Clough GF, Nash K, Hodson L, et al. Effects of purified eicosapentaenoic and docosahexaenoic acids in nonalcoholic fatty liver disease: results from the WELCOME* study. Hepatology. 2014;60(4):1211–21.

50. Nogueira MA, Oliveira CP, Ferreira Alves VA, Stefano JT, Rodrigues LS, Torrinhas RS, et al. Omega-3 polyunsaturated fatty acids in treating non-alcoholic steatohepatitis: a randomized, double-blind, placebo-controlled trial. Clin Nutr. 2016;35(3):578–86.

51. Tanaka N, Sano K, Horiuchi A, Tanaka E, Kiyosawa K, Aoyama T. Highly purified eicosapentaenoic acid treatment improves nonalcoholic steatohepatitis. J Clin Gastroenterol. 2008;42(4):413–8.

52. Sanyal AJ, Abdelmalek MF, Suzuki A, Cummings OW, Chojkier M, EPE-A Study Group. No significant effects of ethyl-eicosapentanoic acid on histologic features of nonalcoholic steatohepatitis in a phase 2 trial. Gastroenterology. 2014;147(2):377–84.

SUPPORTING INFORMATION

Additional supporting information can be found online in the Supporting Information section at the end of this article.